PHOTOGRAPH COURTESY OF © JAREN WILKEY OF BYU PHOTO

Quadrotors and Accelerometers

STATE ESTIMATION WITH AN IMPROVED DYNAMIC MODEL

ROBERT C. LEISHMAN,
JOHN C. MACDONALD JR.,
RANDAL W. BEARD, and
TIMOTHY W. MCLAIN

Quadrotors are ideal platforms for autonomous flight in unknown and complex environments. Their small size and maneuverability are conducive to operating in confined spaces and avoiding obstacles. Equipped with appropriate sensors and algorithms, quadrotors could enable several applications currently infeasible for ground robots.

However, a quadrotor's small size and maneuverability also create problems when attempting to make them autonomous. The same fast dynamics that make

Digital Object Identifier 10.1109/MCS.2013.2287362
Date of publication: 17 January 2014

1066-033X/14/$31.00©2014IEEE

This work has demonstrated improvements in estimation accuracy obtained through a proper understanding of accelerometer measurements and the modeling of rotor drag effects.

quadrotors maneuverable require accurate and frequently updated position, orientation, and velocity state estimates to enable autonomous control. Additionally, the payload available on a quadrotor limits the available sensors and processing capability. These problems are especially relevant in unknown and complex three-dimensional environments that demand more processing-intensive algorithms and information-rich sensor data.

Accurate and timely estimates of attitude and velocity are key ingredients to enable an autonomous quadrotor. In this article, results are presented that quantify how velocity and attitude estimates can benefit from an improvement to the traditional quadrotor dynamic model. The improved model allows accelerometer measurements, which are routinely available at high rates, to reduce an estimator's dependence on complex exteroceptive measurements, such as those obtained by an onboard camera or laser range finder.

A few research groups have made noteworthy progress toward deploying fully autonomous quadrotors. The authors of [1] identify position and velocity estimation as a major challenge. To address this problem, a sophisticated laser scan-matching algorithm was developed. This algorithm is characterized as the key technology that allows the vehicle to fly autonomously.

In [2], a quadrotor system is presented that also uses a scanning laser range finder. The fast vehicle dynamics require pose (that is, position and orientation) estimates with update rates of at least 20 Hz. Several of the design decisions made in the development of this system were driven by the need to meet this requirement despite the system's computational limitations.

An autonomous quadrotor that utilizes the increased information from cameras, at the expense of increased computation, is detailed in [3]. It is emphasized that estimated velocity is critical to damp the system. The estimator relies on a simple constant-velocity motion model that increases the minimum required update rate from the vision processing system.

The widely used traditional quadrotor model (for example, [4]–[11]) assumes that the significant forces acting on the vehicle are gravity and the thrust produced by the rotors (see Figure 1). This assumption leads to a dynamic model for the quadrotor's linear acceleration

$$\begin{bmatrix} \dot{u} \\ \dot{v} \\ \dot{w} \end{bmatrix} = \mathbf{R}_I^b \begin{bmatrix} 0 \\ 0 \\ g \end{bmatrix} + \begin{bmatrix} vr - wq \\ wp - ur \\ uq - vp \end{bmatrix} - \begin{bmatrix} 0 \\ 0 \\ T/m \end{bmatrix}, \tag{1}$$

where p,q, and r are the roll, pitch, and yaw rates of the vehicle, respectively. The components of acceleration along the body-fixed $\vec{i}_b$, $\vec{j}_b$, and $\vec{k}_b$ axes, as shown in Figure 1, are $\dot{u}$, $\dot{v}$, and $\dot{w}$. $\mathbf{R}_I^b$ is the rotation matrix from the inertial to the body-fixed reference frame. The constants g and m represent the gravitational acceleration and the quadrotor's mass. Coriolis forces comprise the second matrix term on the right-hand side of (1). The combined thrust of the rotors, T, acts as an input to the system.

This model is acceptable for some applications, such as designing a controller, because it captures the external forces with the most significant magnitudes. However, the model leads to an interesting paradox [12]. The model implies accelerometers aligned with the $\vec{i}_b$ and $\vec{j}_b$ axes will always measure zero. Yet successful quadrotor implementations with this model use these accelerometer measurements to

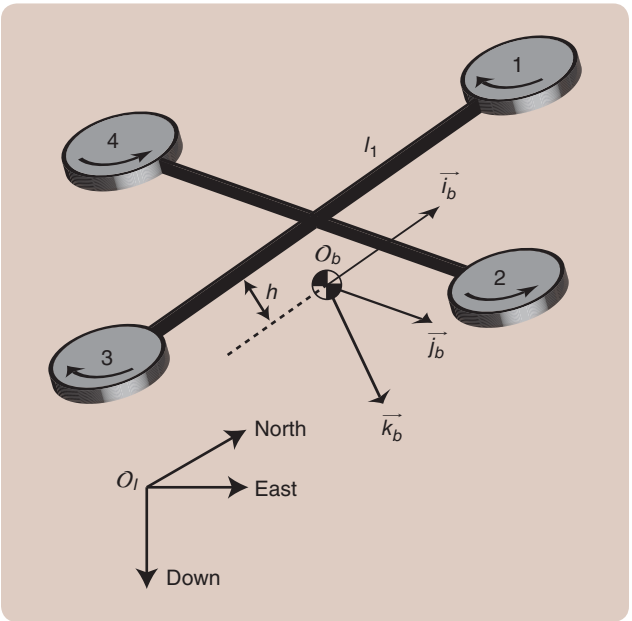

FIGURE 1 The schematic of a quadrotor, showing coordinate frames and notation used in this article. The inertial coordinate frame has its arbitrary origin at O_I with right-hand axes oriented in north, east, and down (that is, aligned with gravity) directions. The body-fixed reference frame has its origin, O_b, at the quadrotor's center of mass, assumed here to be some distance h directly below the quadrotor's geometric center. The body frame $\vec{i}_b$ and $\vec{j}_b$ axes are parallel with the vectors from the geometric center to motors 1 and 2. The $\vec{k}_b$ axis is oriented to complete a right-handed coordinate system. The motors rotate in the directions shown.

In this article, results are presented that quantify how velocity and attitude estimates can benefit from an improvement to the traditional quadrotor dynamic model.

improve estimates of the quadrotor's orientation. An improved quadrotor model should explain how to more appropriately use the data from the accelerometers aligned with the $\vec{i}_b$ and $\vec{j}_b$ axes.

Many articles acknowledge that some drag force must act on the vehicle's body, but this is reasonably dismissed as being small since it is proportional to the square of the vehicle's linear velocity. Other approaches include a drag force that is directly proportional to the quadrotor's linear velocity [13]–[16]. However, the emphasis on control algorithms precludes any discussion of the physics that generate the drag or its effect on accelerometers or the state estimation process. A drag force proportional to linear velocity is included in the estimation approach of [1], based on the observation that something must prevent the quadrotor from accelerating indefinitely. No physical explanation is offered for the effect, and instead a motion-capture system is used to estimate the proportionality constant.

Both [12] and [17] identify a term called *rotor drag* as the force acting in the body-fixed $\vec{i}_b$ and $\vec{j}_b$ axes. Reference [12] derives a dynamic model of the quadrotor from fundamental concepts of blade-element theory, and the rotor drag coefficient for this model is identified from accelerometer measurements. A linearized observer and controller for use with the drag-force-enhanced model is presented and is implemented on an autopilot. The implications of the drag-force model on the control are also explained. The article concludes with a qualitative assessment of how the new model improves the control. However, in [12], the benefits that modeling the rotor drag might bring to state estimation are not examined. Estimated states are not compared to measured values or to results from other standard approaches. Additionally, no information is given on how the drag parameters might be found.

This article builds upon the model derived in [12] and shows specifically how the use of accelerometer measurements in quadrotor flight lead to improved estimation performance. Hardware and truth data confirm that the accelerometers directly measure the translational velocity, allowing more accurate estimates of the attitude and velocity of the vehicle than can be achieved with traditional methods. "An Accelerometer Tutorial" explains why accelerometers in quadrotor flight measure the rotor drag. In several publications, for example, [11], [18], and [19], a subtle mistake is made when relating gravity to the accelerometer measurements on a quadrotor. This article clarifies this issue and shows agreement between the improved accelerometer model and actual measurements.

This new drag-force-enhanced model is easy to use. The drag force constant can be estimated as a state in a filter driven only by inertial measurement unit (IMU) measurements, thus removing the need for experimental tuning, as in [12], or an expensive motion-capture system, as in [1]. Several filters designed to work solely with IMU measurements are presented. To quantify the benefit of the enhanced model in state estimation, the estimates obtained are compared to measurements from a motion-capture system as well as to estimates from more traditional approaches. A two- to threefold improvement in average attitude error is shown, compared to standard approaches. Finally, hardware experiments demonstrate that these performance gains can be maintained far from the near-hover assumption used by [12] in their derivation.

DRAG-FORCE-ENHANCED QUADROTOR MODEL

This section presents a version of the drag-force-enhanced model originally derived in [12]. The derivation begins with employing the assumption of a rigid propeller. The quadrotor is modeled with the nonlinear equations

$$\dot{\mathbf{x}} = \mathbf{f}(\mathbf{x}, \mathbf{u}) + \xi, \tag{2}$$

$$y_i = h_i(\mathbf{x}, \mathbf{u}) + \eta, \qquad i = 1, \ldots, p, \tag{3}$$

where h_i is the ith measurement function, ξ is a zero-mean Gaussian noise term representing unmodeled dynamics with covariance Q, η is the zero-mean Gaussian noise from the sensor with covariance R, and the vector $\mathbf{u}$ represents the inputs that drive the evolution of the estimated states. The inputs are

$$\mathbf{u} = [p \; q \; r]^\top, \tag{4}$$

which are the rotation rates about the $\vec{i}_b$, $\vec{j}_b$, and $\vec{k}_b$ axes, respectively, and correspond to the outputs of the onboard gyroscopes after calibration.

With reference to Figure 1, the states to be estimated are

$$\mathbf{x} = [\phi \quad \theta \quad \psi \quad u \quad v \quad w]^\top, \tag{5}$$

where ϕ, θ, and ψ are the 3-2-1 Euler angles that relate the orientation of the body-fixed frame to the inertial frame, and u, v, and w represent the components of linear velocity in the $\vec{i}_b$, $\vec{j}_b$, and $\vec{k}_b$ axes, respectively.

The drag-force-enhanced model is obtained from (1) by adding a drag force, which is proportional to the body-fixed-frame velocity, to the $\vec{i}_b$ and $\vec{j}_b$ body-fixed components

$$\begin{bmatrix}\dot{u}\\ \dot{v}\\ \dot{w}\end{bmatrix} = \mathbf{R}_I^b\begin{bmatrix}0\\0\\g\end{bmatrix} + \begin{bmatrix}vr-wq\\ wp-ur\\ uq-vp\end{bmatrix} - \begin{bmatrix}0\\0\\T/m\end{bmatrix} - \begin{bmatrix}(\mu/m)u\\ (\mu/m)v\\ 0\end{bmatrix}, \tag{6}$$

where μ is a positive constant. The last term in (6) represents a combination of the profile and induced drag forces on the rotors, which is known in the helicopter literature as the "H-force" or "rotor drag" [20]. In [12], the drag coefficient was modeled as

$$\mu = \lambda_1 \sum_{i=1}^{N} \omega_i, \tag{7}$$

where λ_1 is a positive constant and ω_i is the motor speed of the ith of N motors. However, nominal flight conditions for a quadrotor should dictate that the sum of the motor speeds be nearly constant, resulting in the constant lumped parameter μ in (6). Additional information on using a lumped drag model approach for the rotor drag can be found in [21]. Through extensive flight tests, we have observed that this lumped parameter model holds during nominal flight conditions. This is especially true for autonomous flight using onboard sensors and estimation, where strong accelerations in any direction would degrade camera or laser measurements and make collisions with the environment much more likely.

Using (6), the components of (2) can be expressed as

$$\begin{bmatrix}\dot{\phi}\\ \dot{\theta}\\ \dot{\psi}\end{bmatrix} = \begin{bmatrix}1 & \sin\phi\tan\theta & \cos\phi\tan\theta\\ 0 & \cos\phi & -\sin\phi\\ 0 & \dfrac{\sin\phi}{\cos\theta} & \dfrac{\cos\phi}{\cos\theta}\end{bmatrix}\begin{bmatrix}p\\ q\\ r\end{bmatrix}, \tag{8}$$

$$\begin{bmatrix}\dot{u}\\ \dot{v}\\ \dot{w}\end{bmatrix} = \begin{bmatrix}-g\sin\theta + (vr-wq) - \dfrac{\mu}{m}u\\ g\sin\phi\cos\theta + (wp-ur) - \dfrac{\mu}{m}v\\ g\cos\phi\cos\theta + (uq-vp) - \dfrac{T}{m}\end{bmatrix}. \tag{9}$$

The terms in the first two rows of (9) are due to gravity, Coriolis accelerations, and the drag force. "An Accelerometer Tutorial" shows why gravity is not measured by the accelerometers. In addition, the nonlinear Coriolis terms are assumed small enough to be neglected. Therefore, the $\vec{i}_b$ and $\vec{j}_b$ accelerometer outputs a_{mi} and a_{mj} can be modeled as directly measuring the respective components of the drag force,

$$h_1 \triangleq a_{mi} = \dot{u} + g\sin\theta \approx -\frac{\mu}{m}u, \tag{10}$$

$$h_2 \triangleq a_{mj} = \dot{v} - g\sin\phi\cos\theta \approx -\frac{\mu}{m}v. \tag{11}$$

Equations (10) and (11) are the two measurement functions included in (3) and assume that the accelerometer is located at or near the center of mass.

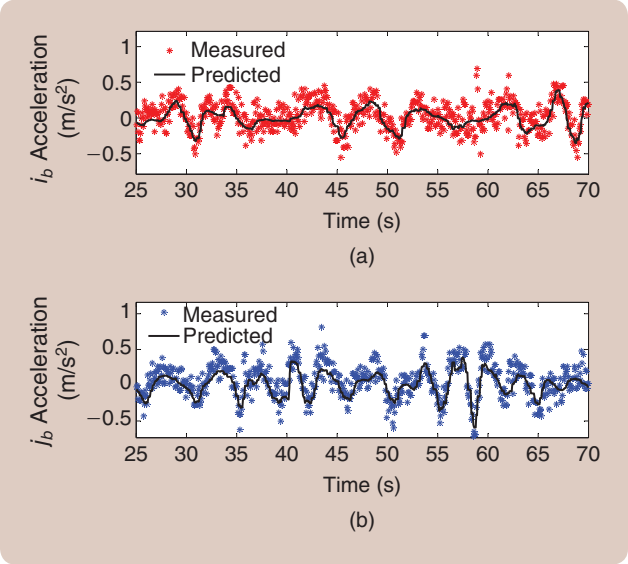

FIGURE 2 The predicted and actual accelerometer measurements. The actual accelerometer measurements for an indoor flight are plotted against those predicted by (10) in (a) and (11) in (b). These plots were generated from time-stamped accelerometer and pose data recorded during a manually controlled flight.

Figure 2 shows the agreement between the actual accelerometer measurements and the predictions of (10) and (11). Figure 2 was generated using recorded time-stamped accelerometer and pose data during a manually controlled flight. Accelerometer measurements came from the onboard sensors and the pose measurements from a motion-capture system. A filtered numerical derivative of the position measurements, expressed in the body-fixed frame of the quadrotor, was used for the u and v velocities in (10) and (11). The value for μ was determined using a least-squares fit of the data from several test flights. The error between the predicted and actual accelerometer measurements is modeled well as zero mean and Gaussian.

WHY THE TRADITIONAL ATTITUDE METHOD ESTIMATES PROVIDE SOME BENEFIT

An alternative to the drag-force enhanced model [12] is to treat estimates as the outputs of a low-pass filter [22]. The system dynamics act as a low-pass filter between changes in attitude and the accelerometer measurements. Using (10) and (11) in (9) and ignoring the Coriolis forces, the time evolution of u and v from (9) can be written as

$$\begin{bmatrix}\dot{u}\\ \dot{v}\end{bmatrix} = \begin{bmatrix}-g\sin\theta - \dfrac{\mu}{m}u\\ g\sin\phi\cos\theta - \dfrac{\mu}{m}v\end{bmatrix}. \tag{12}$$

Consider the first row of (12). Using a small angle approximation and taking the Laplace transform gives the transfer function from θ to u,

An Accelerometer Tutorial

If $\mathbf{a} \in \mathbb{R}^3$ represents the acceleration of a vehicle, m is the mass, and $\mathbf{F}_T \in \mathbb{R}^3$ is the total external force acting on the vehicle, then Newton's second law states that

$$\mathbf{a} = \frac{1}{m}\mathbf{F}_T. \tag{S1}$$

However, accelerometers do not measure the total acceleration $\mathbf{a}$. Accelerometers measure the specific acceleration, meaning the difference between the acceleration of the vehicle and gravitational acceleration.

Figure S1 shows a simplified diagram of a one-axis accelerometer, where a proof mass is attached by a flexure to the housing of the accelerometer. When the proof mass undergoes an acceleration different than the acceleration experienced by the housing, the proof mass deflects and a nonzero measurement is produced. With the accelerometer in Figure S1 on a horizontal surface, the normal force offsets the force due to the weight. The proof mass, which does not experience the normal force, deflects under the influence of gravity, causing the accelerometer to measure an upward acceleration of 1 g. On the other hand, during free fall, gravity would accelerate both the housing and the proof mass, resulting in a measurement of zero.

The output of a three-axis accelerometer mounted on a rigid body is therefore given by

$$\mathbf{a}_m = \frac{1}{m}(\mathbf{F}_T - \mathbf{F}_g), \tag{S2}$$

where $\mathbf{a}_m \in \mathbb{R}^3$ is the measured acceleration and $\mathbf{F}_g \in \mathbb{R}^3$ is the force due to gravity. Equation (S2) states that for an accelerometer to measure the effect of gravity only, all the external forces must sum to zero.

Throughout the article, it is assumed that the axes of the accelerometer are aligned with the body-frame axes and that the accelerometer has been properly calibrated to remove misalignment errors and cross-axis sensitivity.

Below are two different methods for state estimation using accelerometers [12]. Many researchers, for example [27]–[29], have shown that using one of these methods to fuse accelerometers with an exteroceptive sensor increases performance compared to using the exteroceptive sensor alone.

ACCELEROMETER-BASED ATTITUDE ESTIMATION

From (S2), when the sum of external forces is zero, the accelerometers will measure

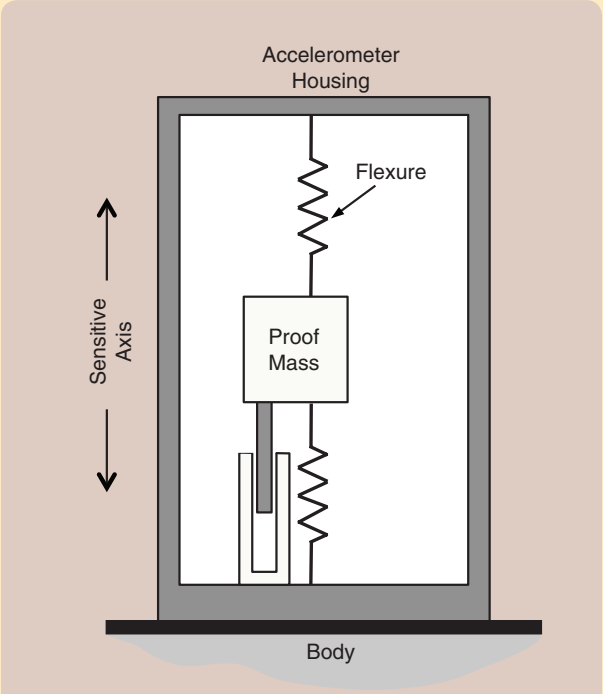

FIGURE S1 A simplified diagram of an accelerometer. When the proof mass undergoes an acceleration that is different than the acceleration experienced by the housing, the proof mass deflects and a nonzero measurement is produced.

$$\mathbf{a}_m = -\frac{1}{m}\mathbf{F}_g. \tag{S3}$$

Let $\mathbf{a}_m^b \triangleq (a_{mi}, a_{mj}, a_{mk})^\top$ represent the acceleration measured in the body-frame axes. In the inertial frame, the force of gravity is $\boldsymbol{F}_g = (0, 0, mg)^\top$. Expressing (S3) in the body frame gives

$$\begin{bmatrix} a_{mi} \\ a_{mj} \\ a_{mk} \end{bmatrix} = \mathbf{R}_I^b \begin{bmatrix} 0 \\ 0 \\ -g \end{bmatrix},$$

$$\begin{bmatrix} a_{mi} \\ a_{mj} \\ a_{mk} \end{bmatrix} = \begin{bmatrix} g\sin\theta \\ -g\sin\phi\cos\theta \\ -g\cos\phi\cos\theta \end{bmatrix},$$

where ϕ is the roll angle and θ is the pitch angle relative to the ground. The roll and pitch angles can therefore be estimated as

$$\hat{\phi}_{\text{accel}} = \tan^{-1}\left(\frac{a_{mj}}{a_{mk}}\right) \tag{S4}$$

$$\hat{\theta}_{\text{accel}} = \sin^{-1}\left(\frac{a_{mj}}{g}\right). \tag{S5}$$

$$u(s) = \frac{\frac{-gm}{\mu}}{\frac{m}{\mu}s + 1}\theta(s). \tag{13}$$

The model for the accelerometer measurement in the $\vec{i}_b$ direction is obtained by substituting (10) into (13) to give

$$a_{mi}(s) = \frac{g}{\frac{m}{\mu}s + 1}\theta(s) \triangleq H(s)\theta(s). \tag{14}$$

By similar arguments, the transfer function for the $\vec{j}_b$ direction is

$$a_{mj}(s) = \frac{-g}{\frac{m}{\mu}s + 1}\phi(s) = -H(s)\phi(s). \tag{15}$$

Equations (14) and (15) describe the first-order response relating the changes in attitude to the accelerometer measurements, where $H(s)$ is a low-pass filter.

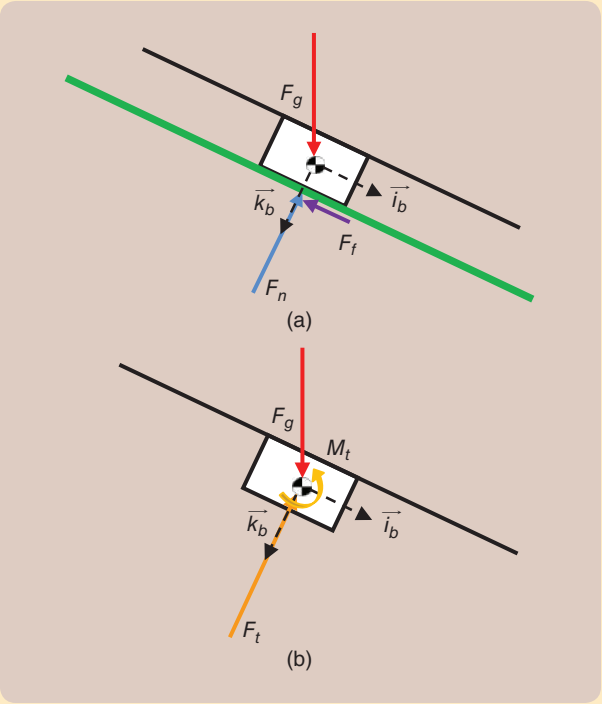

FIGURE S2 Quadrotor free-body diagrams of a quadrotor in two scenarios. Image (a) shows the forces when the quadrotor is sitting on an inclined surface (indicated by the solid green line). Image (b) illustrates the forces according to the standard model when the quadrotor is at a constant attitude in the air and M_t is zero.

This estimation method, expressed by (S4) and (S5), will be termed the *traditional approximation (TA) method*. Note that the underlying assumption of zero external forces is rarely satisfied during quadrotor flight.

ACCELEROMETER-BASED VELOCITY ESTIMATION

If the attitude is known, measured accelerations can be integrated to estimate velocity using

$$\dot{\mathbf{v}}^b = \mathbf{a}_m^b + \frac{1}{m}\mathbf{R}_I^b \mathbf{F}_g, \tag{S6}$$

where $\mathbf{v}^b = (u, v, w)^\top$ is the velocity expressed in the body-fixed frame. This method of using accelerometers is sensitive to the underlying assumption of known attitude. The TA method should not be used to provide the necessary attitude estimates since it requires that $\dot{\mathbf{v}}^b = 0$ The remainder of this article refers to this approach as the *integrated velocity method*.

ACCELEROMETERS ON QUADROTORS

Quadrotors obviously differ from ground vehicles because of the thrust required to keep them airborne. Yet researchers using quadrotors commonly treat them as ground vehicles with respect to accelerometer measurements. Quite often a variant of the TA method provides IMU-based estimates of attitude to a higher-level observer. This second observer then uses the integrated velocity method despite the fact that the underlying assumptions for the two estimators are contradictory.

As a simple example, when a quadrotor rests on an inclined surface, as shown in Figure S2(a), it experiences a normal force $\mathbf{F}_n$, a friction force $\mathbf{F}_f$, and the force due to gravity $\mathbf{F}_g$. The summation of forces in the body frame is

$$\mathbf{F}_T = \mathbf{R}_I^b \mathbf{F}_g - \mathbf{F}_n - \mathbf{F}_f.$$

Consequently, the accelerometer measures

$$\mathbf{a}_m^b = \frac{1}{m}(\mathbf{F}_T - \mathbf{R}_I^b \mathbf{F}_g) = \frac{1}{m}\begin{bmatrix} -F_f \\ 0 \\ -F_n \end{bmatrix},$$

and (S5) can be used to correctly find the pitch angle.

When the quadrotor is in the air with a similar attitude, the forces are usually assumed to be $\mathbf{F}_g$ and the thrust $\mathbf{F}_t$; all other forces are assumed negligible. The thrust force $\mathbf{F}_t$ and moment $\mathbf{M}_t$ are resolved from the individual thrust forces acting at each propeller, which would give the total force, in the body-fixed reference frame, as

$$\mathbf{F}_T \approx -\mathbf{F}_t + \mathbf{R}_I^b \mathbf{F}_g.$$

According to the model, the accelerometers would then measure

$$\mathbf{a}_m^b = \frac{1}{m}(\mathbf{F}_T - \mathbf{R}_I^b \mathbf{F}_g) = \frac{1}{m}\begin{bmatrix} 0 \\ 0 \\ -F_t \end{bmatrix}. \tag{S7}$$

Clearly in this situation, the attitude cannot be determined using (S4) and (S5) since, according to the model, the body frame $\vec{i}$ and $\vec{j}$ accelerometers should always measure zero. It would also be invalid to integrate these values to find the vehicle velocities. Still, many researchers make productive use of the TA and velocity methods within control and estimation schemes. As explained in this article, the discrepancy is due to the rotor drag force that is missing in (S7).

Figure 3 shows the true pitch angle for a quadrotor as measured by a motion-capture system compared to the traditional attitude (TA) estimate described in "An Accelerometer Tutorial," which uses only accelerometer measurements. Superimposed is the result of filtering the true pitch angle with $H(s)$, as given in (14). The TA estimate based on accelerometer measurements agrees well with the low-pass filtered pitch angle.

The TA method given in "An Accelerometer Tutorial" is based on the assumption of static equilibrium. The time constant m/μ governs how quickly the accelerometer measurements react to a step change in the roll or pitch angle. For a heavier quadrotor with $m = 2.75$ kg and $\mu \approx 0.77$, the accelerometer (and therefore the TA estimate) would take more than 10 s to reach 95% of its steady-state value. Even for the more nimble Hummingbird quadrotor

Observability of μ

This sidebar demonstrates the observability of the drag coefficient μ when it is included in the state. Recall that observability is a necessary condition for filter convergence. The theory of nonlinear observability is briefly reviewed. Next, conditions are provided for local observability of the longitudinal quadrotor system with μ included in the vehicle state. This overview is based on a more detailed presentation in [30].

THEORY

Let $\mathbf{x} \in X$, where X is an open subset of $\mathbb{R}^N$, represent the state of the nonlinear system

$$\dot{x} = \mathbf{f}(\mathbf{x}) + \sum_{i=1}^{m} \mathbf{g}_i(\mathbf{x}) u_i, \tag{S8}$$

with n nonlinear outputs of the form

$$y_j = h_j(\mathbf{x}),\ j = 1, \ldots, n, \tag{S9}$$

which form the vector output function $\mathbf{y}(y_1(\mathbf{x}), \ldots, y_n(\mathbf{x}), \mathbf{u})$. Let $S(X)$ and $V(X)$, respectively, designate the set of all scalar-valued smooth functions and the set of all vector fields (that is, column vectors on smooth functions) on X. The functions $\mathbf{f}(\mathbf{x}), \mathbf{g}_i(\mathbf{x}) \in V(X)$ are nonlinear functions of the state and the m time-varying scalars u_i are (known) inputs that drive the system.

Given (S8) and (S9), two states $\mathbf{x}_0$ and $\mathbf{x}_1$ are *distinguishable* if there exists an input function $\mathbf{u}(\cdot)$ such that

$$\mathbf{y}(y_1(\mathbf{x}_0), \ldots, y_n(\mathbf{x}_0), \mathbf{u}) \neq \mathbf{y}(y_1(\mathbf{x}_1), \ldots, y_n(\mathbf{x}_1), \mathbf{u}). \tag{S10}$$

The system is *locally observable* at a point $\mathbf{x}_0 \in X$ if there exists a neighborhood $\mathcal{N}(\mathbf{x}_0)$ around x_0 such that every $\mathbf{x} \in \mathcal{N}(\mathbf{x}_0)$, other than x_0, is distinguishable from x_0. The system is *locally observable* if it is locally observable at each point $\mathbf{x}_0 \in X$.

It can be shown that a system is locally observable at a point $\mathbf{x}_0 \in X$ if there are a sufficient number of linearly independent vectors in the gradients of the measurement equations or the gradients of the Lie derivatives evaluated at $\mathbf{x}_0$. Recall that the Lie derivative of a function $\kappa \in S(X)$ with respect to some vector field $\omega \in V(X)$ is defined by the mapping

$$L_\omega k \triangleq \frac{\partial k(\mathbf{x})}{\partial \mathbf{x}} \cdot \omega(\mathbf{x}) : X \to \mathbb{R}.$$

QUADROTOR LONGITUDINAL STATES WITH μ

The observability of the longitudinal quadrotor system will now be analyzed with μ included in the state. The longitudinal states are $\mathbf{x} = [\theta, u, \mu]^\top$. Recall that θ is the pitch angle, u is the body-fixed forward velocity, and μ is drag coefficient. The longitudinal equations of motion are

$$\begin{bmatrix} \dot{\theta} \\ \dot{u} \\ \dot{\mu} \end{bmatrix} = \mathbf{f}(\mathbf{x}) + u_1 g_1(\mathbf{x}) = \begin{bmatrix} 0 \\ -g \sin(\theta) - \frac{\mu}{m} u \\ s_\mu \end{bmatrix} + u_1 \begin{bmatrix} 1 \\ 0 \\ 0 \end{bmatrix}, \tag{S11}$$

where it is assumed that $\dot{\theta} = q$, the rotation rate about the body $\hat{j}$ axis. The acceleration due to gravity is g, and m is the mass of the vehicle. The time propagation of μ is modeled as a random

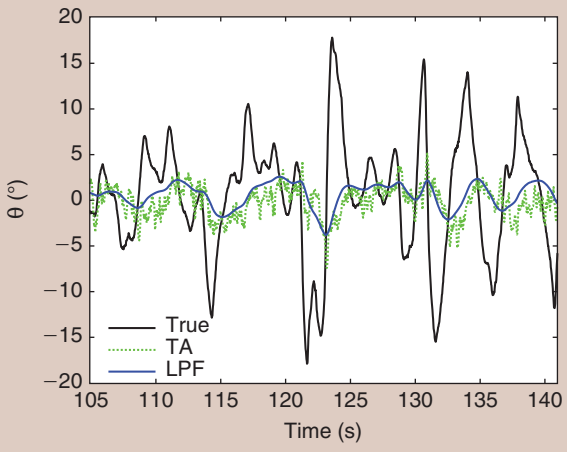

FIGURE 3 A pitch angle comparison of the true pitch angle θ, the traditional attitude (TA) approximation using only accelerometer information, and a low-pass filtered θ for a small portion of a flight. The TA estimation method closely tracks the low-pass filtered pitch angle.

by Ascending Technologies, approximately 3 s would be needed to approach steady state. Long before the accelerometer-based attitude estimate becomes valid, the quadrotor will reach speeds that degrade onboard sensor data or make collision in a cluttered environment likely.

Roll and pitch angle estimates using the traditional approach do not describe fast attitude changes. To compensate, gyroscopes can be used to predict attitude over the short term. Accelerometers are then used to correct the estimates in a measurement update. However, without accounting for the fact that the accelerometers on the quadrotor measure scaled velocities, as shown in (10) and (11), the measurement update will drag the estimates toward the low-pass filtered attitude and not the true attitude. This estimation approach works reasonably well during flights with gradual attitude changes but produces less accurate estimates than are possible by simply including the rotor drag in the model.

OBSERVER DESIGN

This section presents several filter designs using the drag-force-enhanced model for the case where the states

walk where ς_μ is a zero-mean Gaussian random variable. The gyroscope measurement $u_1 = q$ is the input to the system.

The output of the system is the accelerometer measurement in the body $\vec{i}_b$ direction, modeled as

$$y_1 = h_1(\mathbf{x}) = -\frac{\mu}{m}u. \tag{S12}$$

To show that the longitudinal system is locally observable at a point $\mathbf{x}_0 \in X$, there must be three vectors of the observability Grammian that are linearly independent at $\mathbf{x}_0$. The gradient of the output (S12) is

$$\mathbf{d}h1 = \begin{bmatrix} 0 & -\frac{\mu}{m} & -\frac{u}{m} \end{bmatrix}. \tag{S13}$$

Now consider the first-order Lie derivatives. Due to the simplicity of $\boldsymbol{g}_1(\mathbf{x})$ in (S11), $\mathbf{d}L_{g1}h_1 = [0\ 0\ 0]$. The next derivative is

$$\mathbf{d}L_f h_1 = \mathbf{d}\left(\begin{bmatrix} 0 & -\frac{\mu}{m} & -\frac{u}{m} \end{bmatrix}\begin{bmatrix} 0 \\ -g\sin(\theta) - \frac{\mu}{m}u \\ 0 \end{bmatrix}\right)$$

$$\mathbf{d}L_f h_1 = \begin{bmatrix} g\cos(\theta)\frac{\mu}{m} & \left(\frac{\mu}{m}\right)^2 \left(\frac{g\sin(\theta)}{m} + \frac{2\mu u}{m^2}\right) \end{bmatrix}. \tag{S14}$$

The second-order Lie derivative of $\boldsymbol{f}(\mathbf{x})$ is used to find a final vector,

$$\mathbf{d}L_f L_f h_1 = \mathbf{d}\left(\begin{bmatrix} g\cos(\theta)\frac{\mu}{m}\left(\frac{\mu}{m}\right)^2 \frac{g\sin(\theta)}{m} + \frac{2\mu u}{m^2} \end{bmatrix}\begin{bmatrix} 0 \\ -g\sin(\theta) - \frac{\mu}{m}u \\ 0 \end{bmatrix}\right)$$

$$\mathbf{d}L_f L_f h_1 = \begin{bmatrix} -g\cos(\theta)\left(\frac{\mu}{m}\right)^2 & -\left(\frac{\mu}{m}\right)^3 & \left(\frac{-2\mu g\sin(\theta)}{m^2} - \frac{3\mu^2 u}{m^3}\right) \end{bmatrix}. \tag{S15}$$

The vectors (S13)–(S15) are combined into an observability matrix $\boldsymbol{O}_M$ for the longitudinal state,

$$\boldsymbol{O}_M = \begin{bmatrix} 0 & -\frac{\mu}{m} & -\frac{\mu}{m} \\ g\cos(\theta)\frac{\mu}{m} & \left(\frac{\mu}{m}\right)^2 & \frac{g\sin(\theta)}{m} + \frac{2\mu u}{m^2} \\ -g\cos(\theta)\left(\frac{\mu}{m}\right)^2 & -\left(\frac{\mu}{m}\right)^3 & -\frac{2\mu g\sin(\theta)}{m^2} - \frac{3\mu^2 u}{m^3} \end{bmatrix}.$$

The determinant of $\boldsymbol{O}_M$ is

$$|\boldsymbol{O}_M| = -\frac{u\cos(\theta)\mu^4 g + \sin(\theta)m\mu^3 g^2}{m^5}.$$

Since $\mu \neq 0$, the system will be locally observable except when

$$0 = -g\sin(\theta) - \frac{\mu}{m}u. \tag{S16}$$

Equation (S16) is exactly equal to (12) when $\dot{u} = 0$. Consequently, condition (S16) will only be true during unaccelerated flight, as it is then impossible to tell the difference between θ and u, making the state unobservable. Therefore, the longitudinal state $\mathbf{x}$ is locally observable during accelerated, $\dot{u} \neq 0$, flight. The ability to estimate the drag coefficient μ in the state of the vehicle, using only IMU measurements, makes it straightforward to use the drag-force enhanced model for quadrotor state estimation.

$x_{\text{imu}} = [\phi, \theta, u, v]^\top$ are estimated using only IMU data, as is typical on commercially available quadrotor autopilots.

Linear Fixed-Gain Filter

A simple approach to observer design is to make approximations so that the state propagation and measurement equations are linear. In this case, (2) and (3) are replaced by

$$\dot{\mathbf{x}}_{\text{imu}} = \mathbf{A}\mathbf{x}_{\text{imu}} + \mathbf{B}\mathbf{u}, \tag{16}$$

$$\mathbf{y}_{\text{acc}} = \mathbf{C}_{\text{acc}}\mathbf{x}_{\text{imu}}, \tag{17}$$

where $\mathbf{A}$ and $\mathbf{B}$ are the appropriate Jacobians of (8) and (9) and $\mathbf{C}_{\text{acc}}$ is the Jacobian of (10) and (11). The Coriolis forces are assumed to be negligible, and the Jacobians are evaluated at hover. The design is further simplified by choosing a fixed observer gain.

The only outputs of (3) are $\mathbf{y}_{\text{acc}} = [a_{mi}, a_{mj}]^\top$ which are modeled by (10) and (11). With inputs $\mathbf{u} = [p, q, r]^\top$,

$$\mathbf{A} = \begin{bmatrix} 0 & 0 & 0 & 0 \\ 0 & 0 & 0 & 0 \\ 0 & -g & \frac{\mu}{m} & 0 \\ g & 0 & 0 & \frac{\mu}{m} \end{bmatrix}, \tag{18}$$

$$\mathbf{B} = \begin{bmatrix} 1 & 0 & 0 \\ 0 & 1 & 0 \\ 0 & 0 & 0 \\ 0 & 0 & 0 \end{bmatrix}, \tag{19}$$

$$\mathbf{C}_{\text{acc}} = \begin{bmatrix} 0 & 0 & \frac{\mu}{m} & 0 \\ 0 & 0 & 0 & \frac{\mu}{m} \end{bmatrix}. \tag{20}$$

State estimates are propagated using

$$\dot{\mathbf{x}}_{\text{imu}} = \mathbf{A}\mathbf{x}_{\text{imu}} + \mathbf{B}\mathbf{u} + \mathbf{L}_{\text{fg}}\left(\mathbf{y} - \mathbf{C}_{\text{acc}}\,\mathbf{x}_{\text{imu}}\right), \tag{21}$$

where the observer gain $\mathbf{L}_{fg}$ is selected using the *lqr* function in Matlab. Because of its simplicity, this drag-force linear fixed-gain (DFFG) filter is the most practical choice

The assumptions behind the attitude method for measuring the gravity vector are flawed when applied to a quadrotor, even though the approach provides some benefit.

for an embedded processor as opposed to the extended Kalman filters (EKFs) presented below.

EKF with Known μ

The EKF offers improved performance over the linear fixed-gain filter at the expense of increased complexity. Appropriate elements of the nonlinear equations (8) and (9) are used in a separate prediction step to propagate $\mathbf{x}_{\text{imu}}$ forward in time, and Jacobians $\mathbf{A}, \mathbf{B}$, and $\mathbf{C}_{\text{acc}}$ are constantly reevaluated using the current state estimate. This filter is referred to as the drag-force EKF (DF-EKF) in the remainder of the article.

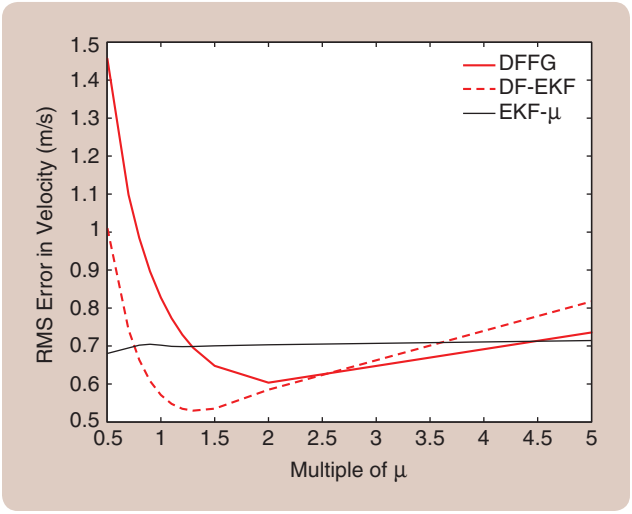

FIGURE 4 Root-mean-square (RMS) errors in velocity for the various drag-force-enhanced filters when the initial estimate of μ is a multiple of the true value. The traditional fixed-gain and nonlinear complementary filters are not shown, as they do not provide a velocity estimate. The drag-force fixed-gain (DFFG) and drag-force extended Kalman filter (DF-EKF) use the initial, but incorrect, value of μ throughout the entire flight. With EKF-μ, the value evolves in time. The DFFG and DF-EKF still provide low RMS values over a wide range of incorrect estimates of μ.

However, the increased complexity arises mainly in maintaining the uncertainty of the state estimates, $\mathbf{P}$, and calculating the variable filter gain. The uncertainty is propagated using

$$\dot{\mathbf{P}} = \mathbf{AP} + \mathbf{PA}^{\top} + \mathbf{BR}_{\text{gyro}}\mathbf{B}^{\top} + \mathbf{Q}. \tag{22}$$

The process uncertainty in (22) is modeled in two parts. The matrix $\mathbf{Q}$ is a hand-tuned diagonal matrix often used only to model the propagation of bias states [23]. Since the inputs $\mathbf{u}$ are gyroscope measurements and $\mathbf{B}$ is the matrix that specifies how the gyroscopes affect the state evolution, $\mathbf{R}_{\text{gyro}}$ is the covariance of the noise on those sensors. Since we can measure the noise characteristics of the gyroscopes, using the $\mathbf{BR}_{\text{gyro}}\mathbf{B}^{\top}$ term makes the filter easy to tune and more accurate than assuming a generic diagonal process noise matrix for all of the states.

The accelerometer measurement update is

$$\begin{aligned}
\mathbf{L} &= \mathbf{P}^{-}\mathbf{C}_{\text{acc}}^{\top}(\mathbf{R}_{\text{accel}} + \mathbf{C}_{\text{acc}}\mathbf{P}^{-}\mathbf{C}_{\text{acc}}^{\top})^{-1},\\
\mathbf{P}^{+} &= (\mathbf{I} - \mathbf{LC}_{\text{acc}})\mathbf{P}^{-},\\
\mathbf{x}_{\text{imu}}^{+} &= \mathbf{x}_{\text{imu}}^{-} + \mathbf{L}(\mathbf{y}_{\text{acc}} - \mathbf{C}_{\text{acc}}\mathbf{x}_{\text{imu}}^{-}).
\end{aligned}$$

The notation Y^{-} and Y^{+} indicates a variable Y before and after the measurement update, $\mathbf{R}_{\text{accel}}$ denotes the covariance

FIGURE 5 A hovering quadrotor from MikroKopter that was used in the experiments. The vehicle is hovering using the measurements from the motion-capture system. (©Jaren Wilkey, BYU Photo.)

FIGURE 6 The motion-capture environment, where all the testing was conducted for this article, uses a motion-capture system from Motion Analysis. The system provides six degrees-of-freedom pose information at 200 Hz with subdegree and submillimeter accuracy.

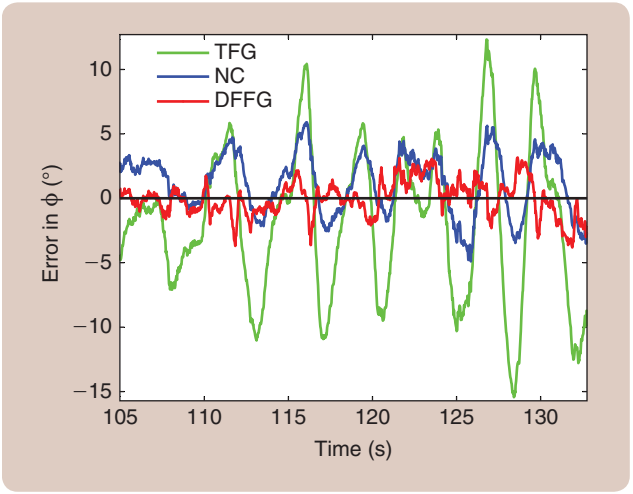

FIGURE 7 The estimation error in roll ϕ. The error in the roll angle over a small window of the manual flight for the traditional fixed-gain (TFG), nonlinear complementary (NC), and drag-force fixed-gain (DFFG) filters. Values closer to zero denote better performance.

of the accelerometer measurement, and $\mathbf{I}$ is an identity matrix of compatible dimensions.

EKF with Estimated μ

The filters given in the previous two sections assume that the rotor drag coefficient μ is known. As a system parameter, μ can be estimated beforehand through a rigorous system identification process using a highly accurate motion-capture system. However, if a motion-capture system is not available, then online estimation of μ is necessary. This section drops assumption that μ is known beforehand and augments the state vector of the EKF so that μ is estimated simultaneously with the other states. It is shown that the parameter can be estimated easily and accurately as part of the state, without the need for motion-capture equipment. Over several different recorded data sets, the filter-estimated value of μ stays within about 5% of the value determined using a motion-capture system. "Observability of μ" shows that μ is observable. In the remainder of the article, the filter derived in this section is designated as EKF-μ.

Estimating μ as a state provides advantages over other approaches that use an improved dynamic model. Reference [12] describes a complicated hand-tuning process that compares estimates from the vehicle to estimates from a global positioning satellite (GPS)-driven attitude heading reference system (AHRS). Since the AHRS cannot be collocated with the vehicle's IMU, the parameter μ must be tuned simultaneously with the position and attitude differences that make the accelerometers on the AHRS agree with the accelerometers of the vehicle. Alternatively, expensive motion-capture equipment and a system identification algorithm can be used to estimate μ [1]. Including μ in the filter state eliminates the need for complicated hand tuning or expensive calibration equipment.

TABLE 1 The root-mean-square (RMS) error for ϕ and θ. The combined RMS errors from the various filters for ϕ and θ from a manual flight.

RMS Error for Attitude Estimates	
Filter	**RMS of ϕ and θ (Degrees)**
Traditional fixed gain	7.27
Nonlinear complementary	5.66
Drag-force linear fixed-gain	2.80
Drag-force EKF	2.16
Drag-force EKF-μ	2.23

Because EKF-μ estimates an additional state, its performance suffers compared to the filters that use a predetermined value for μ. Figure 4 illustrates this point by comparing the root-mean-squared (RMS) error in body-frame velocity over several *initial* values of μ. As expected, EKF-μ is robust to poor initial estimates of μ. If μ cannot be determined by system identification using a motion-capture system or other appropriate sensor, then EKF-μ can be used with manual flight-test data from a quadrotor to provide an estimate of μ. This value for μ can then be used in the standard EKF formulation for subsequent real-time closed-loop flights. The use of EKF-μ over long flight durations may be limited by the accuracy and drift characteristics of the IMU sensors. Figure 4 shows that there is a reasonable range of values for the estimate of μ that enable the fixed-gain and EKF filters to perform well.

IMU-ONLY RESULTS

The MikroKopter [24] quadrotor depicted in Figure 5 and the motion-capture system from Motion Analysis [25] depicted in Figure 6 are used to generate the data. The quadrotor's IMU provides accelerometer and gyroscope measurements at the relatively low rate of 40 Hz. An IMU with a higher data rate could be used but the drag-force-enhanced model enables accurate estimates even from the low-rate data. Pose information for the quadrotor is received from the motion-capture system at 200 Hz. A filtered numerical derivative of the position information is used to estimate the true velocity. All of the data was first recorded from a 250-s manually controlled flight and then processed offline so that comparisons between different filters would be valid.

Comparison Filters

As a baseline to compare against, results are presented from two filters that rely on the TA approach but that add gyroscope measurements. The first is a fixed-gain linear filter described by

$$\dot{\boldsymbol{x}}_n = \begin{bmatrix} p \\ q \end{bmatrix} + \mathbf{L}_n(\mathrm{x}_{\mathrm{accel}} - \mathrm{x}_n), \tag{23}$$

TABLE 2 The root-mean-square (RMS) error on velocity. The combined RMS errors for the velocity estimates *u* and *v* using the drag-force enhanced model. These values are calculated using the data from the entire flight.

RMS Errors for Velocity Estimates	
Filter	**RMS of u and v (m/s)**
Traditional fixed-gain	Not applicable
Nonlinear complementary	Not applicable
Drag-force fixed gain	0.87
Drag-force EKF	0.60
Drag-force EKF-μ	0.67

where $\boldsymbol{x}_n = [\phi, \theta]^\top$. The fixed observer gain $\mathbf{L}_n$ is selected to prevent the estimates from drifting while still tracking fast changes with some accuracy. $\mathbf{L}_n$ was manually tuned to produce results qualitatively similar to those from a popular commercial quadrotor. The parameters were

$$\mathbf{L}_n = \begin{bmatrix} 2.297 & 0 \\ 0 & 2.309 \end{bmatrix}. \tag{24}$$

The vector $\mathbf{x}_{\text{accel}}$ is an estimate of ϕ and θ based on the TA method (S4) and (S5). This filter will be called the traditional fixed-gain (TFG) filter.

The second filter is the explicit nonlinear complementary (NC) filter developed in [26]. This filter estimates the rotation matrix $\hat{\mathbf{R}}$ between the body-fixed reference frame and the inertial reference frame, as well as the biases on the gyroscopes $\hat{\mathbf{b}}$. The filter is implemented using

$$\begin{aligned} \dot{\hat{\mathbf{R}}} &= \hat{\mathbf{R}}((\mathbf{u} - \hat{\mathbf{b}})_\times + k_P(\omega_{\mathbf{mes}})_\times), \ \hat{\mathbf{R}}(0) = \hat{\mathbf{R}}_0 \\ \dot{\hat{\mathbf{b}}} &= -k_I \omega_{\text{mes}} \\ \omega_{\text{mes}} &= \sum_{i=1}^{n} k_i v_i \times \hat{v}_i, \qquad k_i > 0, \end{aligned}$$

where the notation $()_\times$ refers to the matrix form of the cross product, and v_i are vector measurements. Using only IMU information without a magnetometer, there is only one vectorial measurement: the gravity measurement discussed in "An Accelerometer Tutorial." The implementation used in this article was iteratively hand tuned to provide the minimum RMS error in attitude for the data set considered. The gains are $k_P = 0.5$ and $k_I = 0.05$. This filter is called the NC filter in the results section.

Attitude Results

Figure 7 shows the *error* in the estimates for a small portion of the manual flight; results for the pitch angle θ are similar. The figure compares the performance of the TFG and NC filters with the drag-force fixed-gain (DFFG) filter described above.

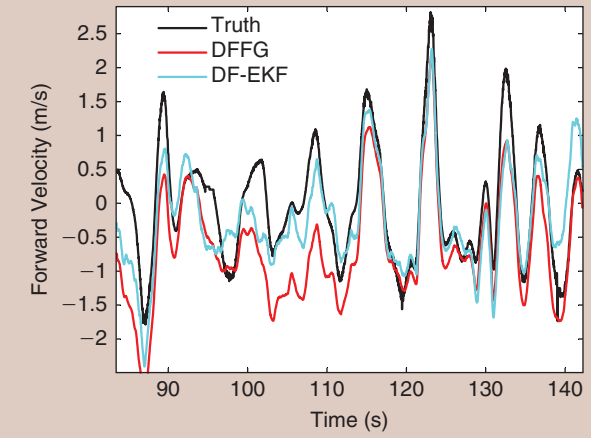

FIGURE 8 The inertial measurement unit (IMU)-only velocity results. Body-frame velocity u truth versus the drag-force fixed-gain filter (DFFG) and extended Kalman filter (DF-EKF) estimates for a small portion of a flight. Velocity estimates are not available when using only IMU data with the traditional fixed-gain and nonlinear complementary filters. Only IMU information is used to produce these estimates.

The filters' performance is further described in Table 1, which presents the RMS error results for all of the filters over the entire flight. DF-EKF and EKF-μ have improved performance over the DFFG filter but at increased computational cost.

Velocity Results

In addition to improving attitude estimates, the enhanced model also provides information on the body-frame velocities u and v that would otherwise be unavailable with IMU-only measurements. Table 2 documents the RMS errors for velocity estimates from the DFFG, DFEKF, and EKF-μ filters over the duration of the flight. Figure 8 illustrates estimates of u produced using the DFFG filter and the DF-EKF (the TFG and NC filters do not provide velocity estimates).

Although the performance does not appear outstanding in Table 2 and Figure 8, note that these results are produced using only inexpensive microelectromechanical system accelerometers and gyroscopes at low data rates. The fact that the improved model offers information on velocity along with high-quality attitude estimates is an additional advantage of the approach. Velocity estimates from the drag-force-enhanced model reduce the rate of required position updates for tradition approaches [23].

Results During Aggressive Maneuvers

The drag-forced enhanced model is robust to aggressive maneuvers, despite the near-hover assumption made in [12] to derive the model. Figure 9 shows estimates of θ for a segment of aggressive flight. The quadrotor experiences pitch

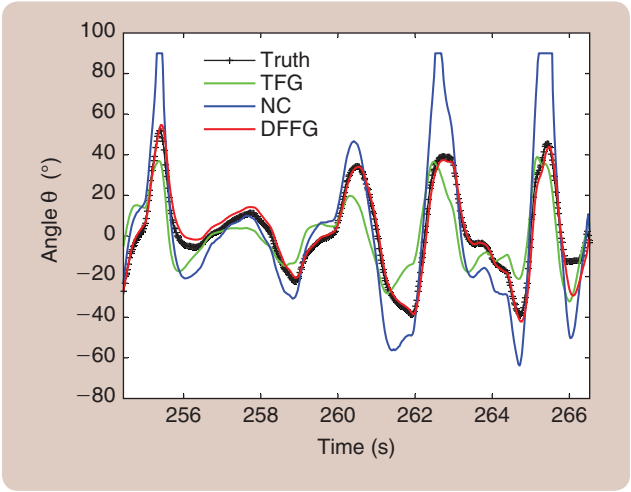

FIGURE 9 The pitch angle during aggressive flight. The true pitch angle θ and its estimates using the traditional fixed-gain (TFG), nonlinear complementary (NC), and drag-force fixed-gain (DFFG) estimators during an aggressive flight are plotted. The DFFG filter provides accurate estimates despite the large angles that are experienced. The filter parameters are identical to those used to produce the previous plots. The saturation in the NC filter are due to the singularity at 90° for a pitch angle. The NC filter was tuned to behave well for nominal flights, but the gains are inadequate for large pitch and roll maneuvers.

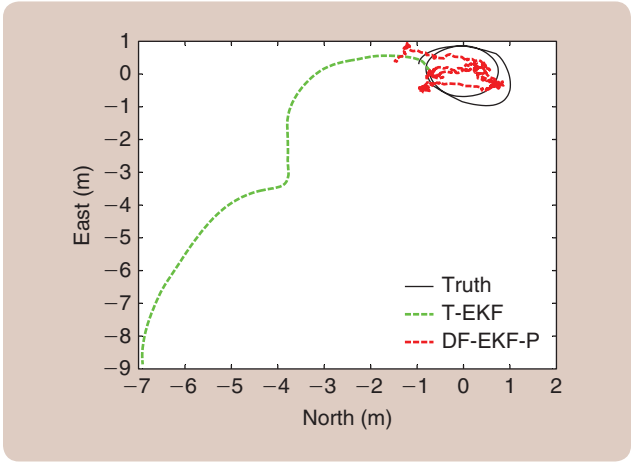

FIGURE 10 Position dead-reckoning results. These position results were obtained using only the inertial measurement unit (IMU) information available from the first 10 s of a manual quadrotor flight. The traditional extended Kalman filter (T-EKF) uses the integrated velocity method mentioned in "An Accelerometer Tutorial" by integrating accelerometer values to obtain position estimates. The drag-force EKF with position (DF-EKF-P) uses the drag-force-enhanced model accelerometer measurement updates to estimate velocity and then integrates the velocity estimates to estimate position. The DF-EKF-P estimates trend with the global position whereas the estimates from the T-EKF approach walk off the chart, which demonstrates the importance of IMU information to the quadrotor state estimates when a valid model is employed.

angles in excess of 45° that are accurately estimated by the drag-force-enhanced model.

The performance improvements shown here are due to the more accurate model of the physical system, which accounts for the rotor drag. The gyroscope measurements provide information for the fast changes in angle and the accelerometer corrections accurately constrain the drift. In the traditional approach, if the gyroscope measurements are trusted too much to track fast angular changes, the attitude estimates drift rapidly. To constrain the drift, the accelerometer measurements must be weighted sufficiently, but using the wrong dynamic model results in inferior performance.

The filter-tuning parameters were not modified for this flight segment, which highlights the robustness of the proposed estimators. The TFG and NC filters could be tuned for better performance during aggressive maneuvers, but then performance near hover would suffer. As an alternative, an adaptive control or gain-scheduling approach could be implemented on those filters to provide improved estimates for a broader flight regime, but at the expense of increased complexity.

Position Dead-Reckoning Results

This section illustrates the significant results possible due to the improved accuracy given by the drag-force-enhanced model. The IMU information was used to dead reckon the quadrotor's global position. This experiment used two filters: the traditional EKF (T-EKF) and the drag-force EKF augmented with position (DF-EKF-P).

The T-EKF is a combination of the two methods presented in "An Accelerometer Tutorial." The TFG filter, explained above, provides the attitude estimates using accelerometer and gyroscope measurements, according to the TA method. Then the filter estimates the global position by integrating accelerometer measurements using the integrated velocity method.

The DF-EKF-P is an augmented version of the DF-EKF, which uses the gyroscopes and accelerometer measurement updates (10) and (11) to estimate the attitude and velocity. The DFEKF-P is augmented to include north and east position states, which are estimated by integrating the velocity estimates.

In both filters, the standard kinematic relationship between velocity and position is used to estimate the position from velocity estimates. Initialization of the position estimates at the starting global location is the only position information provided to either filter during the flight.

Figure 10 shows north and east position dead-reckoning estimates obtained using only the IMU information available during the first 10 s of the quadrotor flight. The DF-EKF-P estimates trend well with the global position whereas the estimates from the T-EKF do not. Figure 11 plots the norm of the north and east error for the T-EKF and the DF-EKF-P. The drift rate is vastly different between the two approaches over the entire flight.

These results demonstrate how much information the IMU can provide to state-estimation algorithms when a

The performance improvements shown here are due to the more accurate model of the physical system, which accounts for the rotor drag.

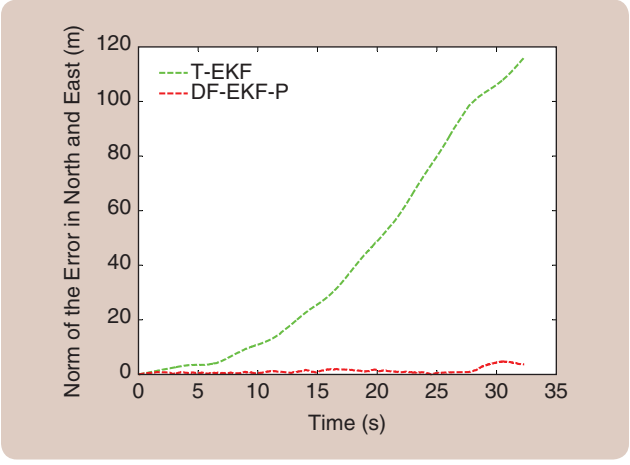

FIGURE 11 ℓ^2 norm of the north and east position errors. The ℓ^2 norm of the north and east dead-reckoning position errors for the traditional extended Kalman filter (T-EKF) and the drag-force EKF with position (DF-EKF-P) are plotted. Inertial measurement unit (IMU) measurements are the only sensor information provided to the two filters. The difference in the drift rate between the two approaches is substantial. Using the DF-EKF-P will allow less-frequent exteroceptive and/or GPS updates because of the much lower drift rate using only the IMU information.

valid model is employed. The basic position information provided by this approach can contribute to a lower dependence on exteroceptive sensor or GPS information [23]. Correctly modeling the accelerometer measurements has a significant impact on position, velocity, and attitude estimates.

CONCLUSION

The assumptions behind the attitude method for measuring the gravity vector are flawed when applied to a quadrotor, even though the approach provides some benefit. When designing an estimator for a quadrotor, the assumption of static equilibrium is too restrictive. The forces acting on the quadrotor will only sum to zero at hover or after a long period of time at a fixed attitude.

Using only IMU data, the EKF and the linear fixed-gain filter based on the drag-force-enhanced model provide a trade-off between complexity and performance. Each filter provides an improvement in attitude estimates compared to typical approaches, even during aggressive maneuvers, while also providing significant information about velocity. The velocity estimates, in turn, can be used effectively by the EKF to provide position estimates based on dead reckoning, which diverges relatively slowly. If μ is unknown, its value can be effectively estimated by its inclusion in the state vector during accelerated manual-controlled flights. The accuracy of the estimates provided from the IMU-only filters could be further improved by increasing the data rate of the IMU.

Future work will include a more extensive study of the constant-μ approximation and the estimation of μ in the state vector. This work has demonstrated improvements in estimation accuracy obtained through a proper understanding of accelerometer measurements and the modeling of rotor drag effects. The lumped-parameter model of rotor drag, though simple, has shown promise for enhanced estimation accuracy and vehicle performance. Additional study of drag effects on small multirotor aircraft may yield additional insights and benefits.

The improvements shown in this article are attributed to the correct characterization of accelerometer measurement, which is a noteworthy advantage as IMU measurements are typically available at high rates and comparatively inexpensive to process.

ACKNOWLEDGMENT

This research is supported through the U.S. Department of Defense SMART Scholarship program: smart.asee.org.

AUTHOR INFORMATION

Robert C. Leishman (robert.leishman@us.af.mil) recently completed the Ph.D. degree in mechanical engineering at Brigham Young University (BYU). He was a recipient of the U.S. Department of Defense Science, Math, and Research for Transformation (SMART) Scholarship. He currently works as a research engineer for the U.S. Air Force Research Laboratory at Wright-Patterson Air Force Base. He received the B.S. degree in mechanical engineering from Utah State University in 2006 and the M.S. degree in mechanical engineering from BYU in 2006. He can be contacted at AFRL/RY, Attn: Robert Leishman, Building 254, Wright-Patterson Air Force Base, OH 45433 USA.

John C. Macdonald Jr. received the B.S. degree in electrical engineering from Brigham Young University in 2002, the M.S. degree in electrical engineering from the Air Force Institute of Technology in 2006, and the Ph.D. degree in electrical engineering from Brigham Young University in 2012. Since February 2013, he has been a research electronics engineer in the U.S. Air Force Research Lab, Sensors Directorate.

Randal W. Beard received the B.S. degree in electrical engineering from the University of Utah, Salt Lake City, in 1991, the M.S. degree in electrical engineering in 1993, the M.S. degree in mathematics in 1994, and the Ph.D. degree in electrical engineering in 1995, all from Rensselaer Polytechnic Institute, Troy, New York. Since 1996, he has been with the Electrical and Computer Engineering Department at Brigham Young University, Provo, Utah, where he is currently a professor. In 1997 and 1998, he was a Summer faculty fellow at the Jet Propulsion Laboratory, California Institute of Technology, Pasadena. In 2006 and 2007 he was a visiting research fellow at the Air Force Research Laboratory, Munitions Directorate, Eglin Air Force Base, Florida. His primary research focus is autonomous control of miniature air vehicles and multivehicle coordination and control. He is a past associate editor for *IEEE Control Systems Magazine* and the *Journal of Intelligent and Robotic Systems* and is currently an associate editor for *IEEE Transactions on Automatic Control*.

Timothy W. McLain is a professor in the Department of Mechanical Engineering at Brigham Young University (BYU). He received the B.S. and M.S. degrees in mechanical engineering from BYU. While completing his Ph.D. work at Stanford University, he worked with the Monterey Bay Aquarium Research Institute on the control of underwater robotic vehicles. He joined BYU in 1995. During the summers of 1999 and 2000, he was a visiting scientist at the Air Force Research Laboratory, where he initiated research on unmanned aircraft, an area on which he continues to focus. With Randal Beard, he is the author of the textbook *Small Unmanned Aircraft: Theory and Practice* (Princeton University Press, 2012). He is currently the director of the Center for Unmanned Aircraft Systems under the National Science Foundation Industry/University Cooperative Research Center program.

REFERENCES

[1] A. Bachrach, S. Prentice, R. He, and N. Roy, "RANGE-robust autonomous navigation in GPS-denied environments," *J. Field Robot.*, vol. 28, no. 5, pp. 644–666, Sept. 2011.

[2] S. Shen, N. Michael, and V. Kumar, "Autonomous multi-floor indoor navigation with a computationally constrained MAV," in *Proc. IEEE Int. Conf. Robotics Automation*, Shanghai, China, May 9–13, 2011, pp. 20–25.

[3] L. Meier, P. Tanskanen, F. Fraundorfer, and M. Pollefeys, "PIXHAWK: A system for autonomous flight using onboard computer vision," in *Proc. IEEE Int. Conf. Robotics Automation*, Shanghai, China, May 9–13, 2011, pp. 2992–2997.

[4] J. P. How, B. Bethke, A. Frank, D. Dale, and J. Vian, "Real-time indoor autonomous vehicle test environment," *IEEE Control Syst. Mag.*, vol. 28, no. 2, pp. 51–64, Apr. 2008.

[5] V. Kumar and N. Michael, "Opportunities and challenges with autonomous micro aerial vehicles," in *Proc. 15th Int. Symp. Robotics Research*, Flagstaff, AZ, Aug. 28–Sept. 1, 2011, pp. 1–16.

[6] M. Hehn and R. D. Andrea, "Quadrotor trajectory generation and control," in *Proc. IFAC World Congress*, Milano, Italy, Aug. 28–Sept. 2, 2011, pp. 1485–1491.

[7] G. Chowdhary, D. M. Sobers Jr., C. Pravitra, A. Wu, C. Christman, H. Hashimoto, C. Ong, R. Kalghatgi, and E. N. Johnson, "Integrated guidance navigation and control for a fully autonomous indoor UAS," in *Proc. AIAA Guidance, Navigation, Control Conf.*, Portland, OR, Aug. 8–11 2011, pp. 1–22.

[8] L. R. G. Carrillo, A. E. D. López, R. Lozano, and C. Pégard, "Combining stereo vision and inertial navigation system for a quad-rotor UAV," *J. Intell. Robotic Syst.*, vol. 65, no. 1–4, pp. 373–387, 2012.

[9] N. Guenard, T. Hamel, and R. Mahony. (2008, Apr.). A practical visual servo control for an unmanned aerial vehicle. *IEEE Trans. Robot.* [Online]. *24(2)*, pp. 331–340. Available: ieeexplore.ieee.org/lpdocs/epic03/wrapper.htm?arnumber=4481181

[10] M. Blosch, S. Weiss, D. Scaramuzza, and R. Siegwart, "Vision based MAV navigation in unknown and unstructured environments," in *Proc. IEEE Int. Conf. Robotics Automation*, Anchorage, AK, May 3–7, 2010, pp. 21–28.

[11] I. Sa and P. Corke, "System identification, estimation and control for a cost effective open-source quadcopter," in *Proc. IEEE Int. Conf. Robotics Automation*, Saint Paul, MN, May 14–18, 2012, pp. 2202–2209.

[12] P. Martin and E. Salaun, "The true role of accelerometer feedback in quadrotor control," in *Proc. IEEE Int. Conf. Robotics Automation*, May 3–7, 2010, pp. 1623–1629.

[13] T. Madani and A. Benallegue, "Backstepping control for a quadrotor helicopter," in *Proc. IEEE/RSJ Int. Conf. Intelligent Robots Systems*, Oct. 9–15, 2006, pp. 3255–3260.

[14] R. Xu and U. Ozguner, "Sliding mode control of a quadrotor helicopter," in *Proc. IEEE Conf. Decision Control*, Dec. 13–15, 2006, pp. 4957–4962.

[15] T. Madani and A. Benallegue, "Control of a quadrotor mini-helicopter via full state backstepping technique," in *Proc. IEEE Conf. Decision Control*, Dec. 13–15 2006, pp. 1515–1520.

[16] S. Bouabdallah, "Design and control of quadrotors with application to autonomous flying," Ph.D. dissertation, École Polytechnique Fédérale de Lausanne, Switzerland, 2007.

[17] A. A. Mian and W. Daobo, "Nonlinear flight control strategy for an underactuated quadrotor aerial robot," in *Proc. IEEE Int. Conf. Networking, Sensing, and Control*, Sanya, China, Apr. 6–8, 2008, pp. 938–942.

[18] L. Meier, P. Tanskanen, F. Fraundorfer, and M. Pollefeys, "PIXHAWK: A system for autonomous flight using onboard computer vision," in *Proc. IEEE Int. Conf. Robotics Automation*, Shanghai, China, May 9–13, 2011, pp. 2992–2997.

[19] S. Grzonka, G. Grisetti, and W. Burgard, "Towards a navigation system for autonomous indoor flying," in *Proc. IEEE Int. Conf. Robotics Automation*, Kobe, Japan, May 12–17, 2009, pp. 2878–2883.

[20] A. R. S. Bramwell, G. Done, and D. Balmford, *Bramwell's Helicopter Dynamics*, 2nd ed. Oxford: Butterworth-Heinemann, 2001.

[21] M. Bangura and R. Mahony, "Nonlinear dynamic modeling for high performance control of a quadrotor," in *Proc. Australasian Conf. Robotics Automation*, Wellington, New Zealand, Dec. 3–5, 2012, pp. 3–5.

[22] C. Chamberlain, "System identification, state estimation, and control of unmanned aerial robots," M.S. thesis, Brigham Young Univ., Provo, UT, Apr. 2011.

[23] J. Macdonald, R. Leishman, R. Beard, and T. McLain, "Analysis of an improved IMU-based observer for multirotor helicopters," *J. Intell. Robotic Syst.*, 2013, doi: 10.1007/s10846-013-9835-5.

[24] Mikrokopter. (2013). [Online]. Available: www.mikrokopter.de/ucwiki/en/MikroKopter

[25] Motion Analysis Corp. (2013). [Online]. Available: www.motionanalysis.com/

[26] R. Mahony, T. Hamel, and J.-M. Pflimlin, "Nonlinear complementary filters on the special orthogonal group," *IEEE Trans. Autom. Contr.*, vol. 53, no. 5, pp. 1203–1218, 2008.

[27] K. Konolige, M. Agrawal, and J. Solá, "Large scale visual odometry for rough terrain," in *Proc. Int. Symp. Robotics Research*, Hiroshima, Japan, Nov. 26–29 2007, pp. 1–12.

[28] P. Piniés, T. Lupton, S. Sukkarieh, and J. D. Tardós, "Inertial aiding of inverse depth SLAM using a monocular camera," in *Proc. IEEE Int. Conf. Robotics Automation*, Rome, Italy, Apr. 10–14, 2007, pp. 2797–2802.

[29] T. Oskiper, Z. Zhu, S. Samarasekera, and R. Kumar, "Visual odometry system using multiple stereo cameras and inertial measurement unit," in *Proc. IEEE Conf. Computer Vision Pattern Recognition*, June 17–22, 2007, pp. 1–8.

[30] M. Vidyasagar, *Nonlinear Systems Analysis*, 2nd ed. Englewood Cliffs, NJ: Prentice-Hall, 1993.